Towards a Precise Measurement of the He^+ 2S Lamb Shift

S. A. Burrows, S. Guérandel, E. A. Hinds, F. Lison*, and M. G. Boshier

SCOAP, University of Sussex, Falmer, Brighton, BN1 9QH, UK

Abstract. We report progress towards making a precise measurement of the 2S Lamb shift in singly-ionised helium by spectroscopy of the 2S–3S transition. The motivation for the experiment is discussed with reference to recent developments in the theory of quantum electrodynamics (QED) and a description of the apparatus and techniques used is given.

1 Introduction

Recent calculations of QED corrections to the Lamb shift in hydrogenic systems have turned out to be rather surprising. In particular, two-loop binding corrections starting in order $m\alpha^2(Z\alpha)^5$ exhibit remarkably non-perturbative behaviour [1,2]. Although up until now measurements in hydrogen have constituted the most accurate tests of bound-state QED, these recently calculated terms are obscured in hydrogen as a consequence of the experimental error in the proton charge radius. The situation in He^+ is more favourable because the alpha particle radius is known well enough to make He^+ Lamb shift measurements sensitive to the two-loop contributions. This is the motivation for our experiment. We are making a precise measurement of the 2S Lamb shift in singly-ionised helium by spectroscopy of the 2S–3S transition. If new measurements confirm the QED theory then existing Lamb shift measurements in hydrogen can be used to determine a new value for the proton charge radius.

2 Overview of Lamb Shift Calculations

Conventionally, the evaluation of bound-state QED corrections is made tractable by including the vacuum fluctuations in several steps. The corrections thus calculated are called *radiative corrections*, and their evaluation can be made by making two expansions. The first is in powers of (α/π) and denotes the number of photon propagator loops present. The second is in the number of photon exchanges with the nucleus and is in powers of $(Z\alpha)$, where Z is the nuclear charge. The expression in equation 1 shows the first two terms of the (α/π) expansion for the case of hydrogenic S-states, i.e. up to two photon loops. In this expression the second expansion has not yet been made and the $(Z\alpha)$ dependence is still contained within the functions F and H.

* Frank.Lison.FL@bayer-ag.de

$$\triangle E(nS) = \; m_e c^2 \frac{\alpha}{\pi} \frac{(Z\alpha)^4}{n^3} F_n(Z\alpha) + m_e c^2 \left(\frac{\alpha}{\pi}\right)^2 \frac{(Z\alpha)^4}{n^3} H_n(Z\alpha) \qquad (1)$$

All the symbols have their usual meanings. In the *non-recoil* limit, the motion of the nucleus is neglected and its finite mass enters only as a reduced mass of the electron. The additional terms arising from the dynamical effects of the nucleus, namely the *recoil corrections* and *radiative-recoil corrections*, have been omitted from equation 1 and will not be considered here. For more detailed discussions of the theory, see the review by Sapirstein and Yennie [3] and more recently [4,5,6]. The expansion in $(Z\alpha)$ is now carried out by expressing F and H as power series in $(Z\alpha)$ and $\ln(Z\alpha)^{-2}$, as shown below in equations 2 and 3, where σ is the ratio of the electron mass to its reduced mass.

$$\begin{aligned} F_n(Z\alpha) \; &= A_{40} + A_{41} \ln[\sigma(Z\alpha)^{-2}] + A_{50}(Z\alpha) \\ &\quad + (Z\alpha)^2 \{A_{60} + A_{61} \ln[\sigma(Z\alpha)^{-2}] + A_{62} \ln^2[\sigma(Z\alpha)^{-2}]\} + ... \end{aligned} \qquad (2)$$

$$\begin{aligned} H_n(Z\alpha) = \; &B_{40} + B_{50}(Z\alpha) \\ &+ (Z\alpha)^2 \{B_{63} \ln^3[\sigma(Z\alpha)^{-2}] + B_{62} \ln^2[\sigma(Z\alpha)^{-2}] + ...\} \; . \end{aligned} \qquad (3)$$

The theoretical value of the 2S Lamb shift in singly-ionised helium presently stands at 13836.7 MHz, with an uncertainty of a few hundred kilohertz. By far the largest contribution to this shift is the one-loop contribution to the self-energy of the electron, which in He^+ accounts for 13614.97 MHz. The mechanism responsible for the shift is the emission and re-absorption of a single virtual photon by the atomic electron, as depicted by the Feynman diagram shown in (a) of Fig. 1. This process contributes to terms A_{40} and A_{41} in the above expansion. It was the one-loop problem that was first calculated in hydrogen by Bethe in 1947, based on non-relativistic QED [7]. The remaining terms in F contain the higher order effects of the nucleus as a (static) source of the Coulomb field, and are called the *binding corrections*. Evaluating these terms requires the consideration of numerous, more complex diagrams and their calculation has involved many physicists and spanned forty years. A review of the methods involved and the earlier results can be found in [3]. The next largest contribution to the Lamb shift comes from the one-loop *vacuum polarisation corrections* to the Coulomb potential, shown in (b) of Fig. 1, at −433.88 MHz in He^+ 2S. This diagram depicts the exchange of a photon between the bound electron and a virtual electron-positron pair which subsequently interacts once with the Coulomb field. In non-field theory terms, this is described as partial screening of the bare charge of the electron by the virtual electron-positron pair, which becomes polarised in the Coulomb field. Heavier pair-produced particles also contribute a small effect (see e.g. [8]).

To further increase the precision of the theoretical determination of the energy levels, it is necessary to add the two-loop terms to the calculation. The

leading order term, B_{40}, was first calculated in 1970, both numerically and analytically [9], and is considered to be well known at 2.037 MHz. It is the next term, the two-loop binding correction, $B_{50}(Z\alpha)$, calculated in 1994 [1] and independently in 1995 [2], which was larger than expected. In He^+ 2S, it contributes -1.339 MHz. Some of the Feynman diagrams which are included in this term are shown in (c) of Fig. 1. The large size of the coefficient B_{50} has prompted debate over the validity of a perturbative approach in the calculation. This debate is further enlivened by the results of several independent calculations [10,11,12,13] of parts of the *perturbed orbital corrections*, which contribute to the B_{50} and the B_{63} terms. Even for hydrogen with its low value of Z, a perturbative calculation to this order means that for the $n = 2$ Lamb shift the first term in the $(Z\alpha)$ power series is essentially cancelled by the second term, despite being of the next order in α. The alternative approach to the calculation involves an exact numerical evaluation of F and H valid for all values of $(Z\alpha)$. At present there is disagreement between the results of these different approaches at the level of a few hundred kilohertz.

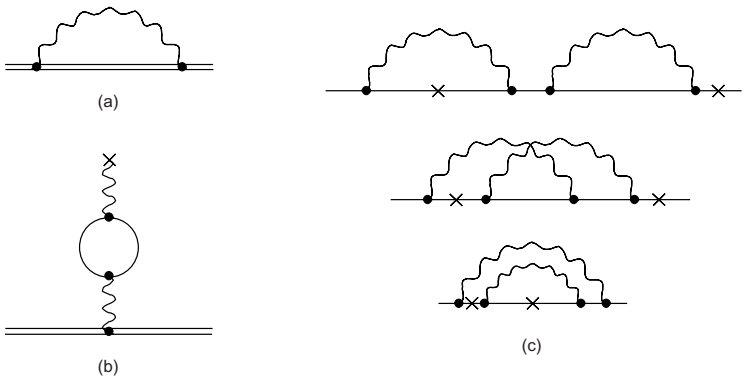

Fig. 1. Feynman diagrams representing various contributions to the Lamb shift. A solid line represents an electron, a wavy line a virtual photon and a cross denotes exchange of a Coulomb photon (**a**) Leading self-energy term (**b**) One-loop vacuum polarisation term. The loop represents a virtual electron-positron pair (**c**) Some diagrams contributing to the two-loop binding correction

Historically, measurements of the 1S Lamb shift in hydrogen have constituted the most accurate tests of bound-state QED. However, these recently calculated terms are obscured in hydrogen by the experimental error in the proton charge radius. This is because a non-QED correction to the Dirac levels due to the finite size of the nucleus is included in the Lamb shift, and the uncertainty in this term for the proton is comparable to the two-loop correction in the 1S state. In He^+, the error introduced by the experimental uncertainty in the alpha particle radius is relatively much smaller [14,15], making Lamb shift measure-

ments in He^+ sensitive to the two-loop binding corrections, which scale with Z^5. In addition, there has not yet been an experiment to measure the He^+ 2S Lamb shift by two-photon spectroscopy . The most precise published experimental value at the time of writing is by van Wijngaarden et al., using the quench anisotropy method [16]. A recent discrepancy between this experiment and the present theoretical number has now been resolved, with the new experimental value of 13836.65(17) MHz [8]. However, it of course remains important to have an independent experimental test of QED at this significant level, particularly one employing a completely different method.

3 The Experimental Method

We are making a precise measurement of the He^+ 2S–3S interval by Doppler-free two-photon spectroscopy of a slow He^+ 2S metastable ion beam, using continuous-wave UV radiation at 328 nm. A measurement of this transition frequency, combined with the value for the Rydberg constant from H experiments, allows a determination of the 2S Lamb shift. See Fig. 2 for the relevant energy levels. The new two-loop corrections amount to a shift in the theoretical value of between −1.3 and −1.5 MHz. This constitutes roughly 10% of the 2S–3S transition natural linewidth, making the experiment potentially a very sensitive test of the theory without the need to identify the centre of the transition to a very small fraction of its width. The experimental difficulties lie in the generation of sufficient quantities of the metastable species and resonant light. Progress to date in these and other aspects of the experiment, depicted schematically in Fig. 3, will be dealt with separately below.

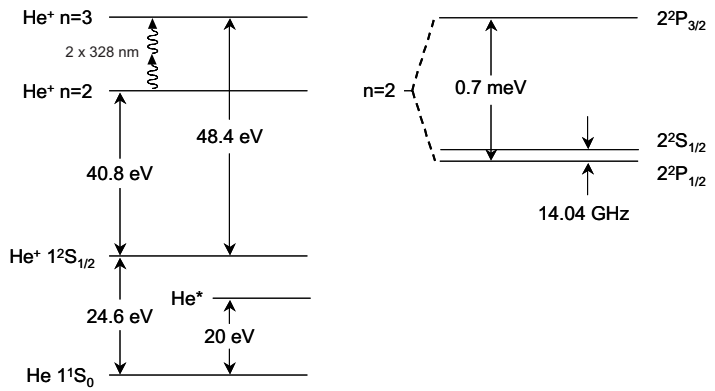

Fig. 2. Low-lying He^+ energy levels relative to the neutral atom ground state, showing the two 2S–3S exciting 328 nm photons. The $n = 2$ Lamb shift and fine structure are shown in the detail. There is no hyperfine structure from the spin-zero ^{4}He nucleus

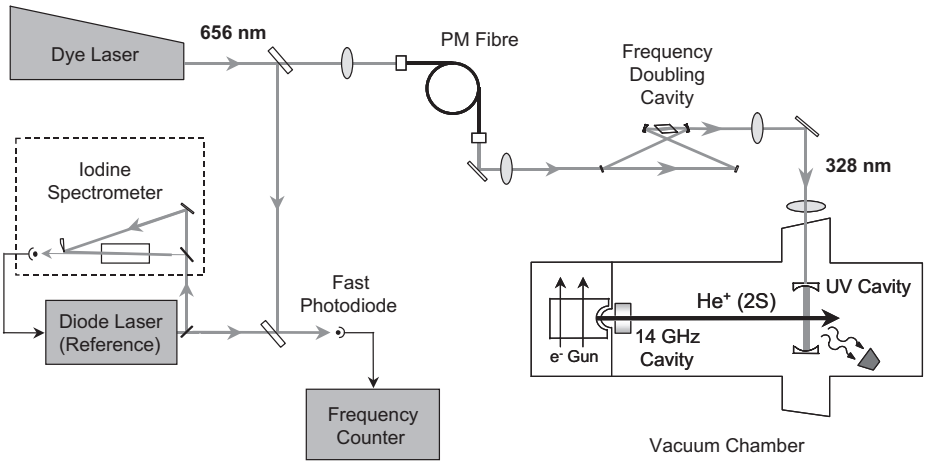

Fig. 3. The experimental setup. A beam of helium metastable ions crosses the resonant light inside a power enhancement cavity, which drives the 2S–3S transition. Note 'PM' denotes polarisation-maintaining

3.1 The UV Light Source

The 2S–3S transition requires the absorption of two 328 nm photons. Because this is a second order process, the transition rate is proportional to the squared intensity of the exciting light. It is therefore desirable to obtain the highest possible light power. A very stable 328 nm c.w. laser has been constructed by frequency doubling the 656 nm light from a dye laser using a BBO crystal in an external enhancement cavity. This comprises a ring cavity based on commercially available optomechanics, consequently care was taken to reduce servo noise due to mechanical resonances in mirror mounts. The cavity is locked on resonance with the fundamental light using the Hänsch–Couillaud polarisation scheme [17]. This source presently generates 70 mW of 328 nm light from about 500 mW of incident 656 nm light. However, this is reduced to around 35 mW with the inclusion of the polarisation-maintaining optical fibre – a necessary addition due to the layout of the experiment. The transfer efficiency through the fibre is about 75%.

3.2 The Interaction Region

The 328 nm light is then coupled into a linear enhancement cavity placed inside the vacuum system. The metastable ions will ultimately be focused through the centre of the resonant mode of the cavity where they will interact with the light. The waist size of the fundamental mode of the cavity is around 100 μm, chosen to make the transit-time broadening roughly equal to the natural width of the transition. A cavity is a convenient way of providing the counter-propagating beams required for the Doppler-free excitation of the two-photon transition,

but its main function is to increase the light power. Without it there would be no hope of obtaining a detectable signal. The power enhancement factor of the cavity (the one-way intra-cavity power on resonance divided by the power incident on the cavity) is measured to be around 90, which means we have over 3 W in each of the counter-propagating beams. This is sufficient for a preliminary experiment, but there is potential for an improvement in this figure given that the finesse of the cavity is around 4000. At present, the efficiency of power coupling into the cavity is limited by the absorptance in the mirrors, which leads to poor impedance matching. A roughly 0.5% reduction of the reflectance of the input coupler would decrease the finesse by a factor of 3 but may increase the theoretical enhancement factor by up to 5, provided it was not accompanied by an increase in absorptance. This would yield a factor 25 increase in 2S–3S excitation rate.

3.3 The He^+ 2S Ion Source and Beam

The hydrogenic $2S_{1/2}$ state is strictly forbidden from decaying by electric dipole transition to the ground state by parity considerations, and so is metastable. The most probable decay route (for low Z atoms) is by the simultaneous emission of two photons, which in the case of He^+ results in a lifetime of 1.9 ms (compared with 140 ms for H). This makes possible a low energy 2S ion beam experiment, which is important if we are to avoid problems with the second order Doppler effect. The metastable He^+ 2S ions are produced in an electron bombardment source of the type used by Hinds et al. [18], which is in operation and is presently being optimised for 2S production. Figure 4 shows a schematic of the source and a photograph of the electron gun arrangement. The electrons are emitted from a large area cathode made of tungsten with a barium impregnant. This is capable of producing half an ampère of emission current when heated to 1100 °C. These electrons are accelerated across a potential difference of 200 V into a molybdenum cage, which forms the anode. A third electrode, the grid, lies between the cathode and the anode, and controls the cathode emission current by building up space-charge in the region in front of the emitting surface. We can thus select an emission of typically tens of mA which, being space-charge-limited by the grid, is insensitive to cathode temperature fluctuations.

The neutral helium atoms are admitted into the source through a pipe connected to a gas bottle outside the vacuum system. Once inside the anode cage they are ionised and excited in a single collision with an electron. The region inside the cage is approximately field-free, which helps to maintain a low energy spread in the final ion beam. An enclosing box, the repeller, is maintained at a positive voltage with respect to the cage to confine the positive ions once produced. Some of the ions drift out of the end of the cage and are extracted by the electrostatic Pierce lens [19] in a direction perpendicular to that of the bombarding electrons. The ions are focused through a channel in the vacuum chamber bulkhead, forming the beam. The beam then passes through a microwave cavity

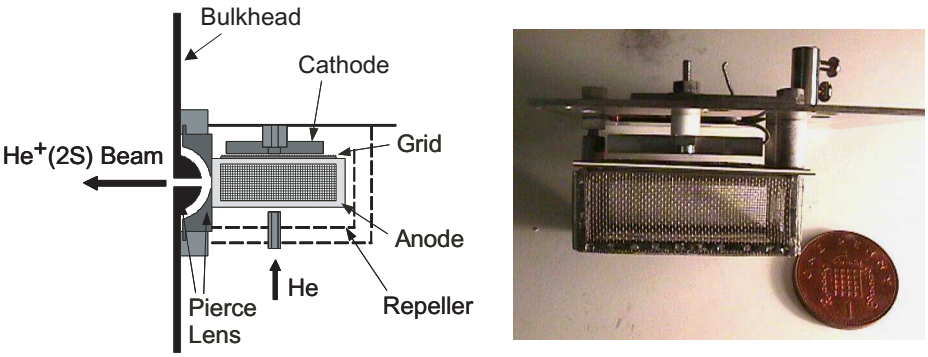

Fig. 4. The ion source and electron gun, shown with penny (20 mm diameter) for scale. Helium atoms in the anode are bombarded by downward-travelling electrons and the ions are extracted horizontally to the left

(described in the following section) and an electrostatic lens system, before finally encountering the UV light. The exact values of electrode potentials inside the source and on the lenses has not yet been finalised, as this is subject to the lens design which is not yet complete. The principle considerations are those of beam divergence and metastable quenching, and since we are interested only in the metastable content of the beam at the UV interaction region, we have to consider the source and lens system as a whole. For example, one may choose to operate the source at a high extraction voltage (the potential between the anode and the bulkhead) and then decelerate the beam through the lens system to give the required 5 eV energy at the UV interaction region. This has the advantages of low beam divergence through the lens and cavity system and prevents space-charge limited flow through the Pierce lens channel. However, too high an electric field in the source increases the probability of Stark quenching of the metastables; the admixture of the $2P_{1/2}$ state introduces a Stark decay rate of $62.5\,E^2\,s^{-1}$ for E in V/cm. A lower extraction voltage does not suffer from this problem but produces a lower total beam current and the slower beam will have larger divergence, leading to greater losses at the beam apertures. Presently we have a 5 eV kinetic energy ion beam, with 55 nA of ion current and about 100 pA of He^+ 2S metastables. The method of detection is described below.

3.4 Metastable Detection

After passing through the UV cavity, the ions are incident on a clean stainless steel plate, which is connected to the input of an electrometer operational amplifier with high current–voltage gain. By applying a positive voltage to the plate we are able to repel the incoming ions and crudely measure their energy distribution. Such a plot is shown in Fig. 5. Applying a negative voltage allows us to distinguish between ground state and 2S metastable ions by means of their different yields for Auger ejection of electrons from the steel surface. The total

current flowing in the electrometer circuit is the sum of the incoming positive ions and the ejected electrons, which are accelerated away from the plate by the bias voltage and thus contribute to the current. The metastables, with an additional 40.8 eV internal energy, have higher yield for the Auger process than the ground state ions (≈0.5 for 2S and 0.2 for 1S) [20] and thus generate a small additional current on the large ground state background. Phase-sensitive detection of this small current is enabled by the microwave cavity. When the cavity is resonantly excited, the intra-cavity power is sufficient to completely quench the metastables by coupling them to the short-lived $2P_{1/2}$ state (this being the method employed by Lamb and Retherford in their historic 1947 experiment). Therefore by modulating the power into the microwave cavity we are able to modulate the metastable content of the beam and correspondingly detect a small AC component of the electrometer current using a lock-in amplifier.

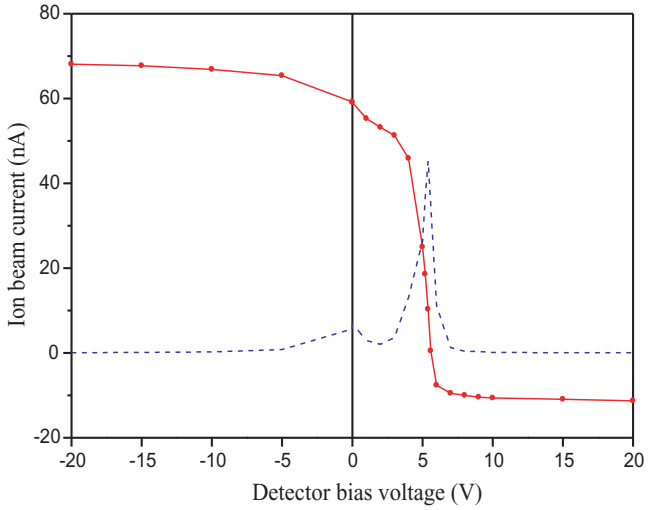

Fig. 5. The solid line with experimental points shows the total ion current collected by the steel plate as its bias is varied. The steep slope of this curve shows clearly that the ions are stopped at about 5 V. The dashed line is the derivative of the solid line and gives the energy distribution of the beam. As the bias goes negative, the secondary electrons liberated by the ion impact are repelled from the plate and appear as a small increase in the total current

The TM_{010} microwave cavity design is very simple, consisting of a cylindrical hollow cut into a block of oxygen-free high-conductance copper, with an end-cap to form a lid. The TM_{010} mode has axial electric field with an antinode on the axis of the cylinder. Beam holes on axis thus allow the $2S_{1/2}$ ions to pass through the highest electric field, which quenches them. The mode frequency, which depends on the cavity radius, is set to the Lamb shift frequency of 14.04 GHz. We

are now making improvements to the cavity, including enlarging the beam holes in order to reduce losses which are presently limiting the ion current.

3.5 The Reference Laser System

A diode laser locked to a hyperfine component of the R(67) 5–5 transition in $^{127}I_2$ will be used as the optical frequency reference at 656 nm. This will be calibrated at the National Physical Laboratory, in the UK, to a precision of around 60 kHz. The absolute frequency of the He^+ transition will be measured by heterodyning light from the reference laser with light from the dye laser on a fast photodiode, as the dye laser is scanned over the 2S–3S resonance. The 2S–3S transition frequency will therefore be measured relative to the calibrated iodine line, as a beat frequency of approximately 1 GHz. The diode laser is used in an external cavity configuration [21], providing over 10 mW single mode operation at 656 nm. Preliminary spectra of the R(67) 5–5 transition taken with 4 mW of diode laser power, are shown in Fig. 6. The laser has yet to be locked and made portable, at which point it will be transported to the NPL for calibration relative to their helium-neon standard. Future generations of the experiment may employ a more sophisticated reference based on the femtosecond comb generator recently developed by Hänsch and co-workers [22].

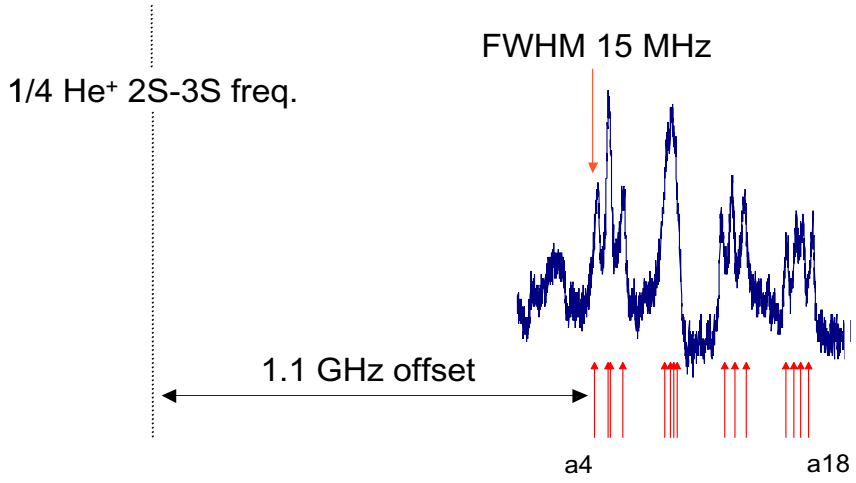

Fig. 6. Experimental spectrum of $^{127}I_2$ shown with calculated hyperfine components a4–a18 of the R(67) 5–5 transition at 656 nm. The a4 component is offset by about 1 GHz from one quarter of the He^+ 2S–3S transition frequency

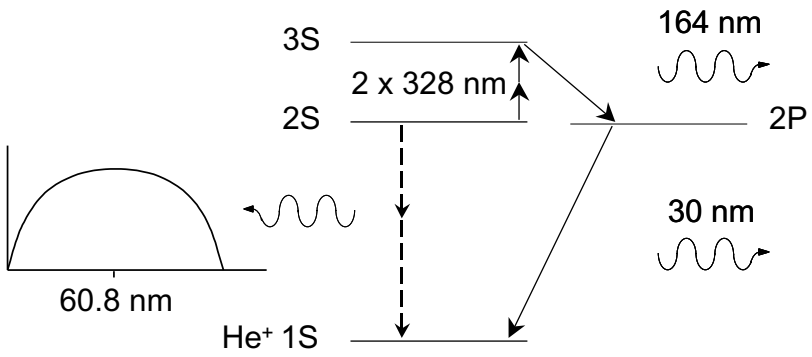

Fig. 7. The 3S-2P-1S decay detection scheme. Detected photons are shown on the right, the dominant background from the 2S 2-photon decay is plotted on the left against frequency

3.6 Detection of the Two-Photon Transition

We will detect the 2S-3S transition by observing fluorescence from the 3S–2P–1S decay cascade, see Fig. 7. The 30 nm radiation may be detected using a channel electron multiplier. The dominant source of background is expected to be from the spontaneous two-photon decay of the metastable state, giving the characteristic broad, symmetrical frequency spectrum centred on 60.8 nm. A thin aluminium filter will be used to suppress this background and eliminate the scattered 328 nm light.

An estimate of the signal to noise from the present figures will be pessimistic as we expect to increase the metastable current by up to an order of magnitude with the changes to the beam discussed above. But with the present laser power and ion current we expect to detect a 2P–1S signal of order 100 counts/s on a background roughly one third this size. This means an integration time of around 0.1 s to give a sensitivity at the level of the two-loop binding corrections and 30 s to achieve a precision limited by the reference laser (∼100 kHz). At this level, the differences between the various calculational methods discussed above will be exposed.

It appears likely that the statistical uncertainty will eventually be reduced to around 100 kHz, so we consider sources of systematic error which may be expected to enter at this level. The uncertainty in the second-order Doppler shift (450 kHz/eV) will be reduced to 100 kHz by a 5% measurement of the beam energy. The AC Stark shift of the 2S–3S transition will be around 70 kHz for the present laser intensity, and can be extrapolated to zero intensity by varying the UV power. Finally, as mentioned above, the systematic uncertainties will be quite different from those in the microwave and quench anisotropy measurements.

4 Conclusion

A determination of the 2S-3S transition frequency to better than 10% of its 16 MHz natural linewidth will be sufficient to probe QED theory at the level of the new two-loop calculations. Once completed, we expect that the present experimental setup will immediately give access to the 100 kHz level, where differences between current calculations can be tested.

5 Acknowledgments

We would like to give thanks to Jörg Werner for work on the iodine-stabilised diode laser. This work is funded by EPSRC.

References

1. K. Pachucki: Phys. Rev. Lett. **72** 3154 (1994)
2. M.I. Eides and V.A. Shelyuto: Phys. Rev. A **52** 954 (1995)
3. J.R. Sapirstein and D.R. Yennie: 'Theory of Hydrogenic Bound States'. In: *Quantum Electrodynamics*, ed. by T. Kinoshita (Singapore, World Scientific 1990) pp. 560–672
4. K. Pachucki et al.: J. Phys. B **29** 177 (1996)
5. S.G. Karshenboim: Can. J. Phys. **77** 241 (1999); V.G. Ivanov and S.G. Karshenboim: this edition, pp. 637–650
6. M.I. Eides et al.: Phys. Rep. in press 2000
7. H.A. Bethe: Phys. Rev. **72** 339 (1947)
8. A. van Wijngaarden et al.: submitted to Phys. Rev. A (2000)
9. T.W. Applequist and S.J. Brodsky: Phys. Rev. A **2** 2293 (1970); B.E. Lautrup et al.: Phys. Lett. **31B** 577 (1970); R. Barbieri et al.: Nuovo Cimento Lett. **3** 588 (1970)
10. S. Mallampalli and J.R. Sapirstein: Phys. Rev. Lett. **80** 5297 (1998)
11. S.G. Karshenboim: JETP **76** 541 (1993)
12. I. Goidenko et al.: Phys. Rev. Lett. **83** 2312 (1999); *this edition*, pp. 619–636
13. V.A. Yerokhin: Phys. Rev. A **62** 012508 (2000); *this edition*, pp. 800–809
14. I. Sick: Phys. Lett. **116B** 212 (1982); I. Sick et al., Phys. Lett. **64B** 33 (1976)
15. C. Ottermann et al.: Nucl. Phys. A **436** 688 (1985)
16. A. van Wijngaarden et al.: Phys. Rev. A **43** 7 (1991)
17. T.W. Hänsch and B. Couillaud: Opt. Comm. **35** 441 (1980)
18. E.A. Hinds et al.: Phys. Rev. A **17** 670 (1978)
19. J.R. Pierce: *Theory and Design of Electron Beams*, 2nd edn. (D. Van Nostrand Co., Inc., Princeton NJ 1954)
20. H.D. Hagstrum.: Phys. Rev. **96** 336 (1954); H.D. Hagstrum and G.E. Becker: Phys. Rev. Lett. **26** 1104 (1971)
21. A.S. Arnold et al.: Rev. Sci. Instrum. **69** 1236 (1998)
22. J. Reichert et al.: Opt. Comm. **172** 59 (1999); F. Biraben, T.W. Hänsch et al.: *this edition*, pp. 17–41